6th European Conference on Computational Mechanics (ECCM 6)
7th European Conference on Computational Fluid Dynamics (ECFD 7)
11 – 15 June 2018, Glasgow, UK

ANOMALY IDENTIFICATION IN MECHANICAL STRUCTURES EXPLOITING THE INVERSE FINITE ELEMENT METHOD

(ECCM –ECFD 2018 CONFERENCE)

L. COLOMBO[1], C. SBARUFATTI[2] AND M. GIGLIO[3]

[1]Politecnico di Milano
via La Masa 1, Milano
luca1.colombo@polimi.it

[2] Politecnico di Milano
via La Masa 1, Milano
claudio.sbarufatti@polimi.it

[3] Politecnico di Milano
via La Masa 1, Milano
marco.giglio@polimi.it

Key words: iFEM, Anomaly Detection, Crack, Damage identification.

Abstract. One main limitation to the implementation of Structural Health Monitoring (SHM) systems in real structures is the influence of different boundary conditions with respect to those adopted during SHM system design, especially for what concerns the loads, potentially leading to damage misclassifications. In this context, the inverse Finite Element Method (iFEM), recently developed for shape sensing of shell structures, can be used to reconstruct the displacement field, thus the strain field, everywhere in a component on the basis of just few strain sensors placed in discrete positions and without requiring any a-priori knowledge of loads or material properties. This work proposes a methodology to perform SHM exploiting the iFEM algorithm for strain reconstruction. In particular, an anomaly index is defined based upon the comparison between the strain read at a target sensor location and the one reconstructed, in the same position, through the iFEM algorithm. When the analyzed structure is in a "healthy" condition, the two values match, otherwise they do not. The defined anomaly index enables to identify both the presence and the position of a defect within the structure without being dependent on the modelled boundary load condition. Computation efficiency is ensured by the iFEM algorithm itself. A very fast reconstruction of the component strain field is achieved once a sensors grid is established within the structure, meaning the method can be easily implemented in an online monitoring system. Though the method formulation is general for an arbitrary component geometry and damage type, the proposed methodology is experimentally tested by means of a clamped plate subjected to fatigue crack propagation. The results underline the method attractiveness for its ability to correctly detect both the presence and the location of the damage without any prior information on the boundary load condition and with a low computational effort.

1 INTRODUCTION

Structural health monitoring (SHM) as a procedure aims at reducing maintenance costs and increasing structural safety in a variety of fields and applications, from mechanical components to big civil infrastructures. In general, SHM infers information about the actual health state of a structure based on a series of data collected by on-board sensors. Information can include the loads acting on the structure [1][2], as well as the damage presence, location and characterization [3].

In this framework, the displacement monitoring, usually referred to as *shape sensing*, covers an important role in the SHM procedure. Among the shape sensing methodologies available in the literature [4][5], the inverse Finite Element Method (iFEM), originally developed by Tessler and Spangler [6][7] for plate and shell structures, stands out for its peculiarities, allowing to reconstruct the deformed shape of a structure on the basis of some strain measurements without any a-priori knowledge of loads or material properties [8][9]. At a glance, it consists in minimizing in a least-squares sense a weighted error functional defined as a comparison between measured and numerically formulated strains. The procedure is computationally efficient, involving mainly matrix-vector multiplication, and fast enough for real-time implementation both in static and dynamic applications [10]. Furthermore, some works in literature confirm the iFEM robustness against noisy measurements [11]. In fact, thanks to intrinsic smoothing operations in the iFEM procedure, an accurate displacement field reconstruction by the algorithm is achieved even in presence of noisy strain measures [12].

Despite the method attractiveness for SHM systems leveraging on strain field measurements [13][14], for which operational variability can dampen damage detection, very few applications of the inverse Finite Element Method to anomaly identification [15] are present in literature. This work exploits the iFEM to define an anomaly index for a model-based damage detection and localization. The anomaly identification relies on the concept that the iFEM will reconstruct a strain field always compatible with the healthy model of the structure. If a non-modelled geometrical modification (e.g. damage) occurs in the monitored structure inducing a strain field perturbation, the iFEM algorithm reconstructs a strain field not representative of the reality in the vicinity of the damage. The proposed methodology is experimentally verified by the authors for a simple plate subjected to fatigue crack propagation, verifying the effect of measurement noise and small model uncertainties on the diagnostic capability.

The paper is structured as follows. The general iFEM framework is briefly described in Section 2. Then, the iFEM output is used in Section 3 to define an anomaly index for damage identification. Section 4 provides information about the specimen under test and the iFEM model for testing the methodology, while detection and localization results are shown in Section 5 for different crack lengths. A conclusive section is finally provided.

2 INVERSE FINITE ELEMENT METHOD OVERVIEW

A brief summary of the iFEM approach to displacement and strain field reconstruction is provided in this section, while a more detailed description can be found in [10][16] for the interested reader.

The iFEM procedure consists in an optimization problem defined as a weighted least-squares variational formulation between measured ($\cdot^{\boldsymbol{\varepsilon}}$) strains and a numerical formulation ($\cdot(\boldsymbol{u})$) of the same, with $\boldsymbol{u}$ referring to the implicit optimization target: the displacement field. Supposing the structure is discretized in shell-like inverse elements, a weighted least-squares functional can be defined for each of them, accounting for membrane ($\boldsymbol{e}$), bending ($\boldsymbol{k}$) and transverse shear ($\boldsymbol{g}$) deformations of the element mid-plane, hereon referred to as reference plane. In particular, for the i^{th} inverse element, the functional takes the form:

$$\Phi_i(\boldsymbol{u}^i) = w_m \left|\left|\boldsymbol{e}(\boldsymbol{u}^i) - \boldsymbol{e}_i^{\boldsymbol{\varepsilon}}\right|\right|^2 + w_b \left|\left|\boldsymbol{k}(\boldsymbol{u}^i) - \boldsymbol{k}_i^{\boldsymbol{\varepsilon}}\right|\right|^2 + w_s \left|\left|\boldsymbol{g}(\boldsymbol{u}^i) - \boldsymbol{g}_i^{\boldsymbol{\varepsilon}}\right|\right|^2 \quad (1)$$

where $\boldsymbol{u}^i$ is the vector of nodal degrees of freedom in local coordinates and w_m, w_b, w_s are positive valued parameters associated to the membrane, bending and shear deformations, controlling the coherence between numerical and measured strains.

Two items are required for the implementation of the iFEM procedure. The first is the numerical formulation of the $\boldsymbol{e}, \boldsymbol{k}, \boldsymbol{g}$ strain components which can be defined following a procedure similar to the direct FEM and not detailed here for brevity. The second is the definition of a vector of input strain measurements ($\boldsymbol{\varepsilon_{in}}$) to be used for defining $\boldsymbol{e}^{\boldsymbol{\varepsilon}}, \boldsymbol{k}^{\boldsymbol{\varepsilon}}, \boldsymbol{g}^{\boldsymbol{\varepsilon}}$. Considering the i^{th} inverse element instrumented with n strain sensors, each measuring 3 strain tensor components and posed at n discrete positions $\boldsymbol{x_j} = (x_j, y_j, \pm h)$ $(j = 1, \dots, n)$ on both the top $(+h)$ and bottom $(-h)$ surfaces, with h referring to the surface distance from the reference plane, the $\boldsymbol{e}$ and $\boldsymbol{k}$ strain components can be computed as:

$$\begin{aligned} \boldsymbol{e}_{i,j}^{\boldsymbol{\varepsilon}} &= \frac{1}{2}\begin{Bmatrix} \varepsilon_{xx}^+ + \varepsilon_{xx}^- \\ \varepsilon_{yy}^+ + \varepsilon_{yy}^- \\ \gamma_{xy}^+ + \gamma_{xy}^- \end{Bmatrix}_{i,j} \\ \boldsymbol{k}_{i,j}^{\boldsymbol{\varepsilon}} &= \frac{1}{2h}\begin{Bmatrix} \varepsilon_{xx}^+ - \varepsilon_{xx}^- \\ \varepsilon_{yy}^+ - \varepsilon_{yy}^- \\ \gamma_{xy}^+ - \gamma_{xy}^- \end{Bmatrix}_{i,j} \end{aligned} \quad (j = 1, \dots, n) \quad (2)$$

The strain component $\boldsymbol{g}$, on the other hand, cannot be directly computed from the measured surface strain components. However, since its contribution can be neglected in most of the engineering applications [16], the $\boldsymbol{g}$ formulation is neglected.

Once the reference plane numerical ($\cdot(\boldsymbol{u})$) and measured ($\cdot^{\boldsymbol{\varepsilon}}$) strain components are defined, a global system of equation can be derived as in eq. (3) by applying a standard finite element procedure to sum up the contribution of each n_{el} element in a single functional and then, minimizing it with respect to the global displacement vector $\boldsymbol{U}$ and applying problem dependent boundary conditions:

$$\boldsymbol{K_{FF}U_F} = \boldsymbol{F_F} \quad (3)$$

After the global displacement field is computed solving eq. (3), a model of the reconstructed strain field ($\boldsymbol{\varepsilon_{iFEM}}$) can be defined through eq. (4):

$$\begin{aligned} \begin{Bmatrix} \varepsilon_{xx} \\ \varepsilon_{yy} \\ \gamma_{xy} \end{Bmatrix} &\equiv \boldsymbol{e}(\boldsymbol{u}^i) + z\boldsymbol{k}(\boldsymbol{u}^i) \\ \begin{Bmatrix} \gamma_{xz} \\ \gamma_{yz} \end{Bmatrix} &\equiv \boldsymbol{g}(\boldsymbol{u}^i) \end{aligned} \quad (4)$$

where z is the through-the-thickness coordinate. A model M_{iFEM} is, thus, available for real-time calculation of the strain field $\boldsymbol{\varepsilon_{iFEM}}$ as a function of $\boldsymbol{\varepsilon_{in}}$ without requiring any a-priori

knowledge of loads or material properties (E, ν) since only strain-displacement relationships are involved in the calculations .

3 IFEM EXPLOITATION FOR DAMAGE IDENTIFICATION

The iFEM model M_{iFEM} for strain field computation ($\boldsymbol{\varepsilon_{iFEM}}$) as a function of $\boldsymbol{\varepsilon_{in}}$ is exploited hereafter for the definition of a synthetic index representative of the health state of the structure and exploitable for determining the damaged area.
The damage identification procedure assumes a defect alters the strain field of a structure with respect to its normal condition. However, the iFEM model (M_{iFEM}) always reconstructs an $\boldsymbol{\varepsilon_{iFEM}}$ compatible with the geometrical discretization of the structure, leading to a discrepancy with the real strain field if the input strain measures $\boldsymbol{\varepsilon_{in}}$ are collected from n_{in} input sensors at $\boldsymbol{x_{in}}$ positions in a damaged component. If a pattern of test strain measures, $\boldsymbol{\varepsilon_t}$, collected from n_t test sensors at $\boldsymbol{x_t}$ positions is available, the structural health state can be inferred by a comparison between the test strain measures $\boldsymbol{\varepsilon_t}$ and the iFEM reconstruction, $\boldsymbol{\varepsilon_{iFEM}}$, in the same $\boldsymbol{x_t}$ test positions. Since in most of the engineering problems a plane strain measure is usually available, allowing the computation of $\varepsilon_{xx}, \varepsilon_{yy}, \gamma_{xy}$ strain components if a strain rosette is used, an equivalent strain $\varepsilon_{eq}: \mathbb{R}^3 \rightarrow \mathbb{R}^1$ is exploited to condensate in a synthetic index all the information available, moving from a comparison in $\mathbb{R}^3$ to one in $\mathbb{R}^1$. In particular, the equivalent strain is selected proportional to second invariant of the deviatoric strain tensor [17], since it synthetizes shape change at constant volume, taking the form:

$$\varepsilon_{eq} = \frac{1}{\sqrt{2}} \cdot \sqrt{\left(\varepsilon_{xx} - \varepsilon_{yy}\right)^2 + \varepsilon_{xx}^2 + \varepsilon_{yy}^2 + 6\gamma_{xy}^2} \tag{5}$$

After evaluating ε_{eq} at $\boldsymbol{x_t}$ positions as a function of $\boldsymbol{\varepsilon_t}$ and $\boldsymbol{\varepsilon_{iFEM}}$, obtaining $\boldsymbol{\varepsilon_{eq,t}} \in \mathbb{R}^{n_t}$ and $\boldsymbol{\varepsilon_{eq,iFEM}} \in \mathbb{R}^{n_t}$ respectively, an anomaly index is computed for each test positions $x_t \subset \boldsymbol{x_t}$ as the percentage difference between $\boldsymbol{\varepsilon_{eq,t}}$ and $\boldsymbol{\varepsilon_{eq,iFEM}}$:

$$i(x_t) = \frac{\varepsilon_{eq,t}(x_t) - \varepsilon_{eq,iFEM}(x_t)}{\varepsilon_{eq,t}(x_t)} \cdot 100 \tag{6}$$

Collecting all the n_t indexes defined in eq. (6) in a vector $\boldsymbol{i}(\boldsymbol{x_t}) \in \mathbb{R}^{n_t}$, the structural health state and the possible damage location can be inferred. For an healthy structure, the vector $\boldsymbol{i}(\boldsymbol{x_t})$ is expected to results in a null vector, $\boldsymbol{i}(\boldsymbol{x_t}) = \boldsymbol{0}$, meaning a perfect correspondence between $\boldsymbol{\varepsilon_{eq,t}}$ and $\boldsymbol{\varepsilon_{eq,iFEM}}$ holds for each test sensor position x_t. On the contrary, for a damaged structure, some deviations from zero will occur in the test positions close to the damage, due to the difference between the reconstructed strain field $\boldsymbol{\varepsilon_{iFEM}}$, always compatible with the healthy structure, and the measured one, $\boldsymbol{\varepsilon_t}$, function of the health state.

The equivalent strain defined in eq. (5) assumes that three strain tensor components are measured at each x_t test sensor position. However, in realistic structures one has to limit the number of measures, possibly measuring just one single strain component (e.g. through fiber optic sensors) in structures possessing preferential load transfer capabilities. In case of mono-axial strain component measurement, the equivalent strain of eq. (5) assumes the trivial form:

$$\varepsilon_{eq} = \varepsilon_{xx} \tag{7}$$

The latter approach is followed in this work demonstrating the method attractiveness for anomaly identification on a simple plate instrumented with a fiber optic system as described hereafter in Section 4.

4 EXPERIMENTAL TEST

An experimental verification of the proposed method for anomaly identification has been performed by means of a simple plate subjected to a fatigue propagation test. In this section a description of the specimen, as well as of the test and the iFEM model are provided.

4.1 The specimen

The approach for damage identification is tested on a clamped plate subjected to a cyclic load in the X direction. The plate has a length of 150 mm, a width of 60 mm and a thickness of 2mm (**Figure *1***).

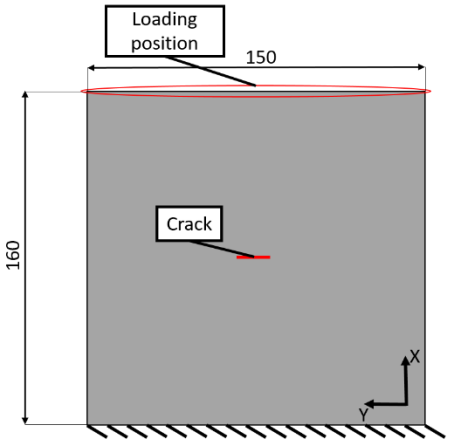

Figure 1: Plate dimensions (mm), boundary condition and crack position

The plate is made of Aluminum 2024 with an elastic modulus of $73\ GPa$ and a Poisson's ratio of 0.33.
The specimen, representative of the plate in ***Figure 1***, is shown in ***Figure 2*** and it is composed by two main parts: (i) the plate and (ii) the gripping system. The latter is used to fix the specimen to the fatigue test machine and to provide an almost uniform load to the upper and lower plate boundaries (***Figure 1***). A $10\ mm$ artificial notch is also created in the middle of the plate to facilitate crack initiation.

As described in Section 3, the damage identification procedure relies on the comparison between the strain measured in some positions and that reconstructed through the iFEM in the same locations. In this work, the applicability of the damage identification procedure is demonstrated with strain measures collected by a Luna fiber optic ODISI B system. This fiber optic technology can provide a very dense measurement path along the optical fiber, thus offering a very high number of available measuring positions within a single cable. Specifically, a $2\ m$ long fiber optic, fixed to the specimen with a DP 490 epoxy glue and possessing measuring points spaced by $2.6\ mm$ from each other, is used in this work to provide the algorithm with both the input ($\boldsymbol{\varepsilon_{in}}$) and test ($\boldsymbol{\varepsilon_{t}}$) strain measures.

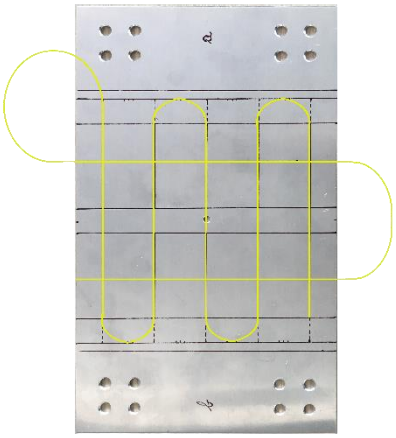

Figure 2: Sensorized specimen

4.2 Test description

The experimental test is performed through an axial fatigue machine MTS Landmark (***Figure 3***) with a maximum force capacity of $100\ kN$.

Figure 3: Detail of the specimen mounted on the MTS Landmark machine; an artificial notch can be noted in the middle of the plate

In order to reduce the amount of data to be analyzed, the strain measures are not collected continuously during the fatigue test but at discrete time instants. For this reason, the test was performed in the following steps: (i) a certain number of cyclic loads in the X direction, with a stress ratio $R = 0.1$ and a maximum load of $15\ kN$, are applied in X-direction to propagate the crack; then, (ii) a static load of $15kN$ is applied in the X direction to open the crack edge, generating the characteristic strain field of a cracked structure and the data for anomaly identification are collected; (iii) finally, the latter are analyzed offline through the in-house developed anomaly identification software.

4.3 The iFEM model and sensor configurations

The last step in the anomaly identification pre-processing procedure requires the definition of the structure geometrical discretization (i.e. mesh, boundary conditions and element connectivity) and of the input ($\boldsymbol{x_{in}}$) and test ($\boldsymbol{x_t}$) strain sensor grids.

The method presented in Section 3 is based on the assumption that a damage alters the strain field within the analyzed structure. A model of a healthy structure produces a discordant output with respect to the real condition if the input is collected from a damaged structure. Since at the beginning of the service life the component can be reasonably assumed to be undamaged, the iFEM model presents no hints of crack presence in the element connectivity, producing a non-matching strain field with the test measures ($\boldsymbol{\varepsilon_t}$) when the real structure is damaged. In particular, only the central part of the specimen in ***Figure 2*** is numerically modelled since the remaining parts serve just as anchoring areas on the axial fatigue machine. The plate is discretized by means of a rather coarse mesh composed by 960 inverse elements with a dimension of 5 mm, thus requiring a very low computational effort in view of a future real-time implementation of the method. As anticipated in Section 2, no material property (E, ν) information is passed to the iFEM, since only strain-displacement relationships are employed in the method.
Two different sensor grids are defined for the input ($\boldsymbol{\varepsilon_{in}}$) and test ($\boldsymbol{\varepsilon_t}$) strains (***Figure 4***). Since, in reality, one is not able to provide each element with a strain measure for technical and practical issues, only some of the inverse elements available are instrumented. In particular, the input grid is composed by sensors placed close to the lateral edges of the specimen measuring along the X direction plus 3 additional sensors within the plate measuring the plate striction (***Figure 4a***), while the test sensors are located in the middle of the plate (***Figure 4b***). Notice that the test sensors configuration is chosen considering sensors whose measures were not corrupted by the acquisition system.
As already anticipated in Section 2, a key step for the iFEM algorithm usage is to convert the input surface measures ($\boldsymbol{\varepsilon_{in}}$) into reference plane strains. Since the experiment was conducted with an axial fatigue machine producing equal strain field on both the plate surfaces, only one face was instrumented, assuming the opposite surface strains equal to the measured ones.

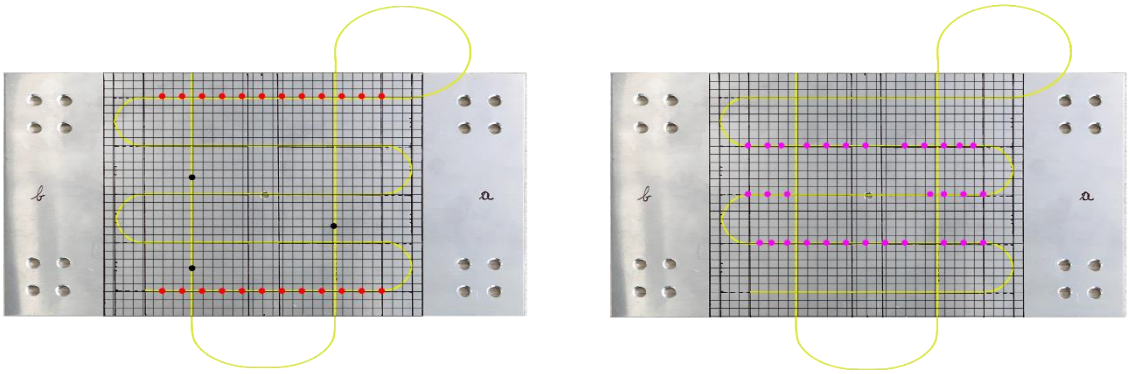

Figure 4: Strain sensor positions along the optical fiber; (a) Input sensors positions ($\boldsymbol{x_{in}}$): in red sensors measuring along the X direction, in black sensors measuring along the Y direction; (b) Test sensors positions ($\boldsymbol{x_t}$)

5 RESULTS

The damage identification outcomes for the clamped plate described in Section 4.1 and subject to a fatigue crack propagation are presented in this section. Subplots in ***Figure 5*** present the anomaly index results, computed for each test positions, for different crack lengths. The same color scale for all the subplots is used in order to facilitate understanding the effect of the damage extension on the method.

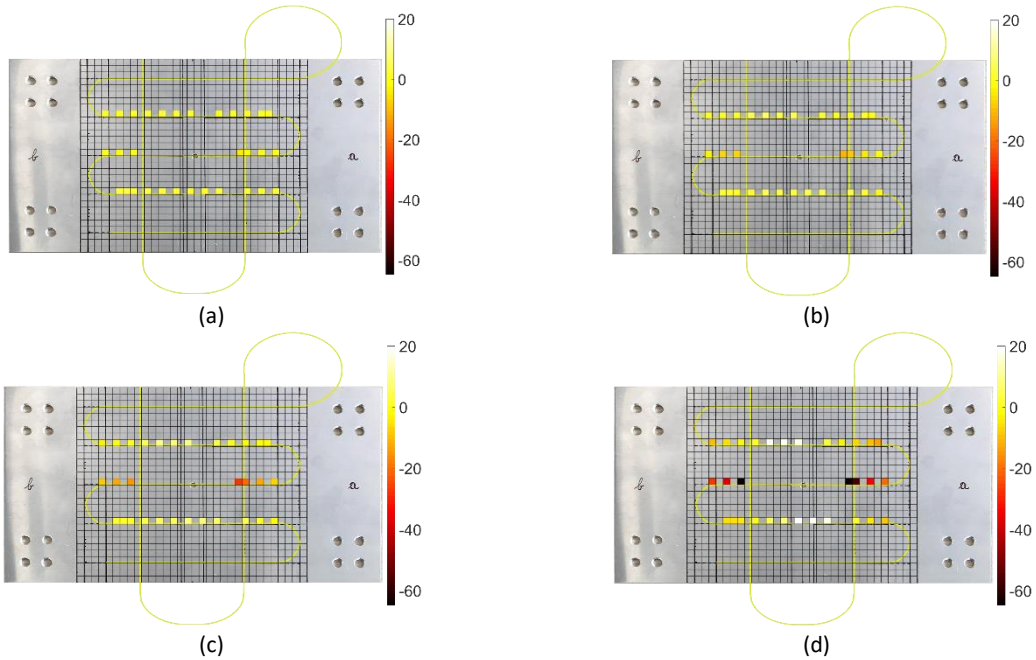

Figure 5: Anomaly index computed under different crack lengths; (a) crack of 3.83 *mm*; (b) crack of 9.38 *mm* (c) crack of 18.81 *mm*; (d) crack of 30.71 *mm*. The crack is always located in the center of the plate, with orientation as in ***Figure 1***.

Table 1: Peak value of the anomaly index (in magnitude) for different crack lengths

Crack length (mm)	Anomaly index peak value in magnitude (%)
3.83	4.1683
5.61	6.9943
7.1	9.7268
9.38	11.5628
15.53	20.1481
18.81	27.2939
22.19	36.4573
26.8	56.5510
30.71	72.4956

The peak values (in magnitude) of the anomaly index are also reported in **Table 1** for increasing crack lengths. As described in Section 4.1 an artificial notch was created to facilitate crack initiation, thus, in order to appreciate just the effect of crack growth on the anomaly index, the results are cleaned from the influence of the artificial notch. First, it can be appreciated the high damage sensitivity of the index, reflected in a significant variability of the index with respect to the undamaged situation in which its values are close to zero. In fact, with the target sensors grid of ***Figure 4b***, the index is able to detect a damage due to a crack with a length of just about $4\ mm$. Furthermore, the results in ***Figure 5*** clearly point out the method possesses a quite extended detection area. Indeed, a significant peak change in the index values with respect to the normal condition, denoting the presence of a defect, is found despite the closest sensor is located at a remarkable distance from the damage, thanks to the peculiar strain field perturbation due to presence of the crack.

Second, the index correlation to the damage size can be recognized. The greater the crack length, the greater the anomaly index peak, moving from a value of about $4.2\ \%$ with a crack length less than $4\ mm$, up to a value of about $72.5\ \%$ when the crack length is about $31\ mm$. Moreover, since the index is normalized by the load through the strain (eq.(6)), for a given type of load (e.g. axial load), it is only function of the actual health state of the structure.

Finally, the index distribution in ***Figure 5*** suggests the possibility of exploiting the anomaly index also for damage localization. In fact, considering the fiber optic layout within the plate, the peak magnitude of the index is found in the closest location with respect to the crack edge. The latter consideration means that, given a test sensors grid is properly designed for the particular application and as a function of the desired sensitivity, the anomaly index can be also exploited for determining the position of a possible damage within a structural component.

6 CONCLUSIONS

In this work, a new feature for anomaly identification is defined based on the inverse Finite Element Method. The iFEM ability to reconstruct the strain field of a structure as a function of discrete strain measurements without requiring any a priori knowledge of the applied load and material properties is exploited to define a strain-based damage sensitive feature easily implementable in damage identification scenarios.

An anomaly index is defined as the percentage difference between an equivalent strain calculated from a strain measure at a test sensor position and the one computed through the iFEM strain reconstruction in the same location. For a properly discretized healthy structure the two equivalent strains match, generating a pattern of zero valued anomaly indices in the test positions. On the contrary, a modification in the real strain field due to a defect is reflected in a mismatch between the two parameters, leading the anomaly index to largely differ from zero in the test positions close to the damage.

The experimental results confirm the validity of the proposed method. A significant sensitivity to a fatigue crack defect is noticed in a clamped plate subjected to a fatigue crack propagation test, reflected in a significant peak value deviation from zero, the latter representing the baseline

healthy condition. Furthermore, for a given type of load, the index is only function of the actual health state of the structure with increasing peak value as a function of the damage size. The index distribution within the plate suggests also a possible exploitation for damage localization, with the peak value found in correspondence of the closest position to the defect considering the fiber optic disposal within the component. The method robustness against noisy measures is also positively confirmed. Indeed, intrinsic smoothing procedures, included in the iFEM procedure facilitating displacement reconstruction, allow a good strain field reconstruction also with noisy measurements.

Despite the results presented in this work are obtained with a reduced form of the equivalent strain, since the tested plate was instrumented with a mono-axial strain sensor (i.e. optical fiber) thanks to a preferential load transfer capability, the method can be also implemented with an extended version leveraging on the equivalent strain, if more complex load configurations are applied. Indeed, though not reported here being matter of present and future research by the authors, if three strain tensor components are measured, e.g. through a strain rosette, a load-adaptive baseline can be defined, meaning a feature insensitive to operational variations can be easily created, further increasing the method attractiveness for more complex geometries and load conditions.

REFERENCES

[1] R. Fuentes, E. Cross, A. Halfpenny, K. Worden, and R. J. Barthorpe, "Aircraft parametric structural load monitoring using Gaussian process regression," in *7th European Workshop on Structural Health Monitoring, EWSHM 2014 - 2nd European Conference of the Prognostics and Health Management (PHM) Society*, 2014, pp. 1933–1940.

[2] A. Airoldi, L. Marelli, P. Bettini, G. Sala, and A. Apicella, "Strain field reconstruction on composite spars based on the identification of equivalent load conditions," in *Proceedings of SPIE - The International Society for Optical Engineering*, 2017, vol. 10168.

[3] C. Sbarufatti, A. Manes, and M. Giglio, "Performance optimization of a diagnostic system based upon a simulated strain field for fatigue damage characterization," *Mech. Syst. Signal Process.*, vol. 40, no. 2, pp. 667–690, 2013.

[4] L.-H. Kang, D.-K. Kim, and J.-H. Han, "Estimation of dynamic structural displacements using fiber Bragg grating strain sensors," *J. Sound Vib.*, vol. 305, no. 3, pp. 534–542, 2007.

[5] M. A. Davis, A. D. Kersey, J. Sirkis, and E. J. Friebele, "Shape and vibration mode sensing using a fiber optic Bragg grating array," *Smart Mater. Struct.*, vol. 5, no. 6, pp. 759–765, 1996.

[6] A. Tessler and J. L. Spangler, "A variational principle for reconstruction of elastic deformations in shear deformable plates and shells," *NASA/TM-2003-212445*, 2003.

[7] A. Tessler and J. L. Spangler, "Inverse FEM for full-field reconstruction of elastic deformations in shear deformable plates and shells," in *2nd European Workshop on Structural Health Monitoring; 7-9 Jul. 2004; Munich; Germany*, 2004.

[8] M. Gherlone, P. Cerracchio, M. Mattone, M. Di Sciuva, and A. Tessler, "Shape sensing of 3D frame structures using an inverse finite element method," *Int. J. Solids Struct.*, vol. 49, no. 22, pp. 3100–3112, 2012.

[9] M. Gherlone, P. Cerracchio, M. Mattone, M. Di Sciuva, and A. Tessler, "An inverse finite element method for beam shape sensing: theoretical framework and experimental validation," *Smart Mater. Struct.*, vol. 23, no. 4, p. 45027, 2014.

[10] A. Tessler and J. L. Spangler, "A least-squares variational method for full-field reconstruction of elastic deformations in shear-deformable plates and shells," *Comput. Methods Appl. Mech. Eng.*, vol. 194, no. 2–5, pp. 327–339, 2005.

[11] A. Kefal, J. B. Mayang, E. Oterkus, and M. Yildiz, "Three dimensional shape and stress monitoring of

bulk carriers based on iFEM methodology," *Ocean Eng.*, vol. 147, pp. 256–267, 2018.
[12] A. Tessler, "Structural analysis methods for structural health management of future aerospace vehicles," in *Key Engineering Materials*, 2007, vol. 347, pp. 57–66.
[13] C. Sbarufatti and M. Giglio, "Performance qualification of an on-board model-based diagnostic system for fatigue crack monitoring," *J. Am. Helicopter Soc.*, vol. 62, no. 4, pp. 1–10, 2017.
[14] C. E. Katsikeros and G. N. Labeas, "Development and validation of a strain-based structural health monitoring system," *Mech. Syst. Signal Process.*, vol. 23, no. 2, pp. 372–383, 2009.
[15] C. Quach, S. Vazquez, A. Tessler, J. Moore, E. Cooper, and J. Spangler, "Structural anomaly detection using fiber optic sensors and inverse finite element method," in *AIAA Guidance, Navigation, and Control Conference and Exhibit*, 2005, p. 6357.
[16] A. Kefal, E. Oterkus, A. Tessler, and J. L. Spangler, "A quadrilateral inverse-shell element with drilling degrees of freedom for shape sensing and structural health monitoring," *Eng. Sci. Technol. an Int. J.*, vol. 19, no. 3, pp. 1299–1313, 2016.
[17] G. T. Mase, R. E. Smelser, and G. E. Mase, *Continuum mechanics for engineers*. CRC press, 2009.